

STEADY-STATE CRACKING IN BRITTLE SUBSTRATES BENEATH ADHERENT FILMS

ZHIGANG SUO and JOHN W. HUTCHINSON

Division of Applied Sciences, Harvard University, Cambridge, MA 02138, U.S.A.

(Received 16 September 1988)

Abstract—A crack in a brittle substrate parallel to the film/substrate interface is considered. Stress intensity factors are obtained as a function of film/substrate thickness, elastic properties and edge loads at arbitrary crack depth. These results, combined with the criterion $K_{II} = 0$, are used to predict the steady-state cracking depth. The critical combination of residual stress and film thickness below which steady-state substrate cracking is avoided can be inferred provided the substrate toughness is known.

1. INTRODUCTION

Today's technology demands devices joined by many combinations of structural material groups (ceramics, metals, polymers). The evaluation and enhancement of the mechanical reliability of these inhomogeneous structures have emerged as high priority subjects to both the materials science and solid mechanics communities. Cracking and decohesion processes in film/substrate systems have been studied extensively in recent years. The cracking path and pattern vary substantially for different film/substrate systems with different relative fracture resistances of film, substrate and interface, sign of the residual stress, etc. When films are exposed to residual compression, there are two main ways in which failures can occur: films may buckle from substrates and delaminate (Evans and Hutchinson, 1984; Argon *et al.*, 1989); or substrates may split along the direction perpendicular to the interfaces (Gruninger *et al.*, 1987). For films under residual tension, decohesion can initiate at the edges of the specimen, or at an internal crack in the film, running along the interface at first, and then either continue to propagate along the interface if the interface has low enough toughness or deviate into the substrate if its toughness is sufficiently low. The interfacial cracking process in film/substrate systems is beginning to be understood. Some recent efforts in this direction can be found in Argon *et al.* (1989), Charalambides *et al.* (1989), Kim and Jiang (1986) and Suo and Hutchinson (1989a, b). Some remarkable photographs of cracking in films are presented in Argon *et al.* (1989), where an amorphous SiC coating is deposited on a Si single crystal wafer with (100) surface and where cracks run away from the initial flaw through the coating parallel to the two $\langle 110 \rangle$ directions. These directions are the stiffest in the plane of the (100) wafer and thus produce the largest tensile misfit stress across them in the coating. Most observed failure modes and the present status of understanding have been reviewed in a recent article by Evans *et al.* (1988).

In the present paper, attention will be focused on the cracking process in brittle substrates. Experiments have revealed that cracks in films exposed to residual tension have a strong tendency to extend into brittle substrates and evolve into a trajectory parallel to the interface (Cannon *et al.*, 1986; Hu *et al.*, 1988; Thouless *et al.*, 1987; Drory *et al.*, 1988). This is not an uncommon phenomenon. For a system (Fig. 1) consisting of a thin

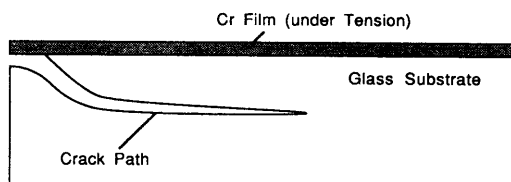


Fig. 1. A schematic drawing of cracking trajectory.

Cr film (under tension) deposited on a glass substrate (Hu *et al.*, 1988), for example, the crack initiates at the edge of the specimen, extends along the interface for about 1–2 film thickness and then deviates into the substrate and propagates parallel to the interface at a depth of 4–5 film thicknesses beneath the interface. The initial stage of the process is rather complicated to characterize, although attempts to model the initial kinking out of the interface have been made in He and Hutchinson (1989). However, the striking feature that the crack does tend to run parallel to the interface at some characteristic depth has been understood owing to systematic efforts combining experiments and theoretical analyses cited above. In these investigations, observed crack depths were compared with the theoretical predictions based on the criterion that a crack seeks a depth where $K_{II} = 0$, and a close correlation for many material couples over a wide range of film/substrate thickness was found. The object of this paper is to predict the steady-state cracking depth for various film/substrate systems under general edge loading (residual stress is equivalent to a particular combination of edge loads), and provide the information on the critical combination of film thickness and external loads below which delamination by substrate cracking can be inhibited.

In the next section, both stress intensity factors K_I and K_{II} are computed for a crack at *arbitrary* depth parallel to the interface. In Section 3 an equation governing the steady-state cracking depth under general edge loads is obtained by enforcing $K_{II} = 0$. In particular, films subject to residual tension are investigated in detail. The steady-state cracking depth, and the associated parameter $\Omega = K_I/\sigma\sqrt{h}$, referred to as the *decohesion number* (Evans *et al.*, 1988), where σ is the residual tensile misfit stress in the film and h the film thickness, are presented for various film/substrate thicknesses and elastic moduli. The latter, in conjunction with the knowledge of the substrate toughness K_{Ic} , provides the critical combination $\sigma\sqrt{h}$ below which steady-state substrate cracking is avoided. In the final section, two competing crack paths in film/substrate systems are considered. A criterion is proposed to predict the tendency of a film/substrate system exposed to misfit tensile stress in the film to undergo interface cracking in preference to substrate cracking or vice versa.

2. STRESS INTENSITY FACTORS

The basic plane elasticity problem which is analyzed is depicted in Fig. 2a. The system consists of a thin film of material No. 1 deposited on a substrate of material No. 2. Each material is taken to be isotropic and linearly elastic. A crack parallel to the interface is pre-existing in the substrate. The problem is asymptotic in that the two material layers are infinitely long and the crack is semi-infinite. The structure far ahead and behind the crack tip is considered as three (composite) beams, with longitudinal load P_i and moment M_i per unit thickness acting at the neutral axis of each of them. No residual stress is present at this stage of development. However, it will be shown in the next section that the residual stress is equivalent to a particular combination of edge loads. Various length quantities specified in Fig. 2a are normalized by the film thickness, h , with λ as relative cracking depth and λ_0 as substrate/film thickness ratio. The two parameters, Δ and Δ_0 , measuring the levels of the neutral axes, depend on λ and λ_0 and elastic properties, and expressions for them are given in Appendix A. The task below is to relate the stress intensity factors, K_I and K_{II} , to the external loads, P s and M s, as well as to h , λ_0 , λ , and the elastic moduli of the two materials. It should be emphasized that the solution is quite sensitive to the substrate thickness (measured by λ_0) even for very thin films, contrary, perhaps, to one's intuition. In the first collaborated attempt to understand the phenomenon of substrate cracking (Thouless *et al.*, 1987), the comparison, which gave rise to appreciable discrepancies, was made between a theoretical prediction based on the solution for an infinitely thick substrate and the experimental data obtained, of course, for a finite substrate. These discrepancies were removed later by considering substrates with finite thickness using finite element calculations (Drory *et al.*, 1988).

The nondimensional elastic moduli dependence of bimaterial systems, for traction-prescribed boundary value problems, may be expressed in terms of two Dundurs' (1969) parameters

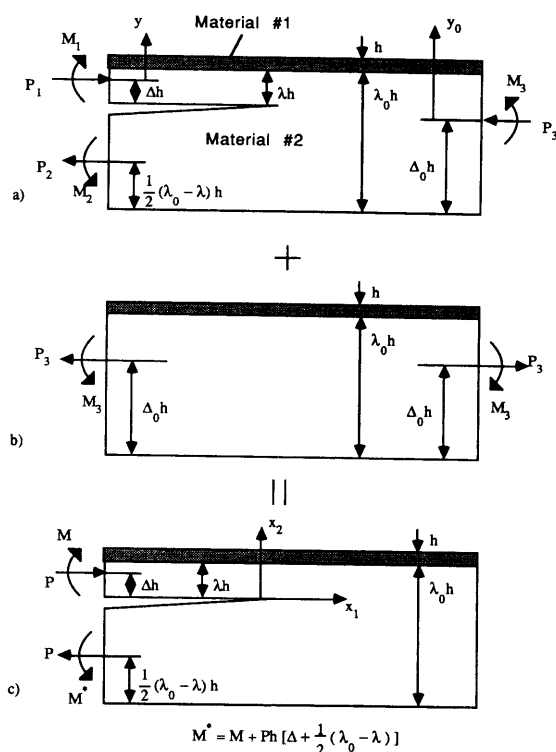


Fig. 2. Conventions and geometry.

$$\alpha = \frac{\Gamma(\kappa_2 + 1) - (\kappa_1 + 1)}{\Gamma(\kappa_2 + 1) + (\kappa_1 + 1)}, \quad \beta = \frac{\Gamma(\kappa_2 - 1) - (\kappa_1 - 1)}{\Gamma(\kappa_2 + 1) + (\kappa_1 + 1)}. \quad (1)$$

Subscripts 1 and 2 refer to the two materials in Fig. 2a, $\kappa = 3 - 4\nu$ for plane strain and $(3 - \nu)/(1 + \nu)$ for plane stress, $\Gamma = \mu_1/\mu_2$, ν is Poisson's ratio and μ is the shear modulus. The physically admissible values of α and β are restricted to a parallelogram enclosed by $\alpha = \pm 1$ and $\alpha - 4\beta = \pm 1$ in the α, β -plane. The two parameters measure the elastic dissimilarity of two materials in the sense that both vanish when the dissimilarity does. Two other bimaterial parameters, Σ , the stiffness ratio, and ε , the oscillatory index, are related to α and β , respectively, by

$$\Sigma = \frac{c_2}{c_1} = \frac{1 + \alpha}{1 - \alpha}, \quad \varepsilon = \frac{1}{2\pi} \ln \frac{1 - \beta}{1 + \beta} \quad (2)$$

where $c = (\kappa + 1)/\mu$. Thus α can be readily interpreted as a measure of the dissimilarity in stiffness of the two materials. Material No. 1 is stiffer than No. 2 as $\alpha > 0$ and material No. 1 is relatively compliant as $\alpha < 0$. The parameter ε , thus β , as has been discussed extensively in the literature on interfacial fracture mechanics, is responsible for the oscillatory behavior at an interfacial crack tip. However, it will be apparent later that for the problem considered now, with the crack tip in a homogeneous material, the solution depends weakly on β . Hence for many practical applications, taking $\beta = 0$ can be a very good approximation.

Overall equilibrium requires that the six loads in Fig. 2a satisfy

$$\begin{aligned} P_1 - P_2 - P_3 &= 0 \\ M_2 + M_3 - M_1 - P_1 h (\Delta + \lambda_0/2 - \lambda/2) + P_3 h (\Delta_0 - \lambda_0/2 + \lambda/2) &= 0. \end{aligned} \quad (3)$$

Therefore only four among the six are independent, say, P_1 , P_3 , M_1 and M_3 . Superposing the solution for the composite beam in Fig. 2b onto that for the structure in Fig. 2a, one

finds that the number of load parameters controlling the crack tip singularity can be reduced to two, i.e. P and M in Fig. 2c, given by

$$P = P_1 - C_1 P_3 - C_2 \frac{M_3}{h}, \quad M = M_1 - C_3 M_3 \quad (4)$$

where the nondimensional numbers, C_s , are given in Appendix A. It is the reduced problem in Fig. 2c that will be analyzed below. Once the solution is obtained, the solution to the general problem in Fig. 2a can be readily constructed by reinterpreting P and M via (4).

In the following the functional form of the stress intensity factors, K_I and K_{II} , of the system in Fig. 2c is sought. It is worthwhile to bear in mind that the solution in general should depend on P , M , h , c_2 (or c_1) and dimensionless parameters λ_0 , λ , α and β .

The energy release rate can be calculated exactly by using the strain energy stored in the structure per unit width per unit length far behind the crack tip. The result is a positive definite quadratic in P and M which can be written as

$$G = \frac{c_2}{16} \left[\frac{P^2}{Uh} + \frac{M^2}{Vh^3} + 2 \frac{PM}{\sqrt{UV}h^2} \sin \gamma \right] \quad (5)$$

where U and V are dimensionless positive numbers and the angle γ is restricted to the range $|\gamma| < \pi/2$ for definiteness. Expressions for these quantities can be found in Appendix A. Notice that all the nondimensional quantities appearing in (4) and (5) depend only on λ_0 , λ and Σ (thus α), but not on β . This clearly indicates that the energy release rate for the general problem in Fig. 2a is β -independent.

The stress intensity factors, K_I and K_{II} , depend linearly on P and M , which, in conjunction with dimensional analysis, dictates the functional form

$$K_I + iK_{II} = \frac{1}{\sqrt{2}} \left[a \frac{P}{\sqrt{Uh}} + b \frac{M}{\sqrt{Vh^3}} \right] \quad (6)$$

where $i = \sqrt{-1}$ and a and b are nondimensional complex numbers depending on α , β , λ and λ_0 . Furthermore, since the energy release rate is related to the stress intensity factors by

$$G = \frac{c_2}{8} (K_I^2 + K_{II}^2), \quad (7)$$

comparison of eqns (5) and (6) reveals that the numbers must satisfy

$$|a| = 1, \quad |b| = 1, \quad \bar{a}b + a\bar{b} = 2 \sin \gamma. \quad (8)$$

Equation (8) provides three constraints among two complex numbers. Hence only one real quantity is undetermined, which is introduced as ω , such that

$$a = e^{i\omega}, \quad b = -ie^{i(\omega + \gamma)}. \quad (9)$$

The angle ω only depends on α , β , λ and λ_0 , and will be calculated and discussed shortly. Now it is possible to rewrite (6) more explicitly as

$$K_I + iK_{II} = \frac{1}{\sqrt{2}} \left[\frac{P}{\sqrt{Uh}} - ie^{i\gamma} \frac{M}{\sqrt{Vh^3}} \right] e^{i\omega} \quad (10)$$

or

Table 1. $\omega(\alpha, \beta, \lambda_0 = \infty, \lambda)$ (in degrees)

α β λ	-.8		-.6		-.4		-.2		0.0		0.2		0.4		0.6		0.8	
	-4	0.0	-4	0.0	-3	0.1	-3	0.1	-2	0.2	-2	0.2	-1	0.3	-1	0.3	0.0	0.4
0.1	45.7	44.3	46.4	45.4	47.6	47.5	49.7	49.8	51.8	53.1	54.6	56.4	58.0	61.3	61.9	66.0	68.5	75.3
0.5	54.9	52.4	55.6	52.0	54.7	51.1	55.1	51.0	54.2	50.5	54.9	51.0	54.8	51.4	56.9	53.5	60.3	58.0
1	54.4	53.1	55.2	53.2	54.7	52.5	54.6	51.9	53.5	50.8	53.2	50.1	52.2	49.2	52.5	49.1	53.3	50.0
1.5	53.5	52.9	54.2	53.1	54.1	52.7	53.9	52.2	53.0	51.2	52.4	50.3	51.2	48.9	50.5	47.8	49.7	46.8
2	53.1	52.7	53.6	52.9	53.5	52.6	53.4	52.3	52.7	51.4	52.1	50.5	50.8	49.1	49.6	47.6	47.8	45.5
3	52.6	52.4	52.8	52.5	52.9	52.5	52.8	52.3	52.4	51.7	51.7	50.9	50.6	49.7	49.1	47.9	46.4	44.9
4	52.3	52.4	52.5	52.4	52.6	52.4	52.5	52.2	52.2	51.8	51.7	51.2	50.6	50.0	49.2	48.4	46.2	45.1
5	52.3	52.2	52.4	52.3	52.5	52.3	52.4	52.3	52.2	52.0	51.8	51.5	50.9	50.5	49.4	48.9	46.4	45.6
6	52.2	52.2	52.3	52.3	52.4	52.3	52.3	52.2	52.2	52.0	51.8	51.6	51.0	50.8	49.6	49.3	46.7	46.1
10	52.1	52.1	52.1	52.1	52.1	52.1	52.1	52.1	52.0	52.0	51.8	51.7	51.4	51.3	50.4	50.2	47.9	47.7

$$K_I = \frac{P}{\sqrt{2Uh}} \cos \omega + \frac{M}{\sqrt{2Vh^3}} \sin (\omega + \gamma)$$

$$K_{II} = \frac{P}{\sqrt{2Uh}} \sin \omega - \frac{M}{\sqrt{2Vh^3}} \cos (\omega + \gamma) \quad (11)$$

so that the stress intensity factors are fully determined apart from the single dimensionless real function $\omega(\alpha, \beta, \lambda_0, \lambda)$. From (11) one can restrict ω to the range $0 < \omega < \pi/2$ to recover the positive signs of K_I and K_{II} as anticipated for the special case $P > 0$ but $M = 0$. It is significant to note that of the two parameters, α and β , characterizing the elastic dissimilarity of two materials, α is by far the more important one, since β enters the formulation only through ω , and it will be clear soon that ω depends weakly on β . Moreover, detailed calculations below show that ω is *almost invariant* over wide ranges of the parameters α , β , λ_0 and λ . A proposal of taking $\omega = 52^\circ$ will be made for the situations where only crude estimates are desired.

Specific determination of the function $\omega(\alpha, \beta, \lambda_0, \lambda)$ requires that the crack problem be rigorously solved for one loading case for a given structure, i.e. prescribed values of α , β , λ and λ_0 . This has been done in Appendix B by solving the integral equation based on continuously distributed edge dislocations. The function $\omega(\alpha, \beta, \lambda_0, \lambda)$ is listed in Tables 1 and 2 at $\lambda_0 = \infty$, 10, respectively, for various α and some extreme values of β , at several selected cracking depths λ . The dependence of ω on the four variables is relatively weak. It is believed that ω is analytic in $1/\lambda_0$ for large λ_0 , and therefore ω can be well approximated by linear interpolation in $1/\lambda_0$ between $1/\lambda_0 = 0$ and 0.1, where values of ω have been tabulated. Since β enters the stress intensity factors formulae (11) only through ω , and from Tables 1 and 2 one knows that ω is a very weak function of β , it is apparent that taking $\beta = 0$ can be a very good approximation for many applications. For this purpose we have listed more extensively the values of ω at $1/\lambda_0 = 0$, 0.05, 0.1, for various α and λ in Tables 3, 4 and 5, all with $\beta = 0$.

Contact can be made with some earlier works. For a thin film bonded on a semi-infinite substrate, that is $\lambda_0 = \infty$, eqn (11) is reduced to

Table 2. $\omega(\alpha, \beta, \lambda_0 = 10, \lambda)$ (in degrees)

α β λ	-.8		-.6		-.4		-.2		0.0		0.2		0.4		0.6		0.8	
	-4	0.0	-4	0.0	-3	0.1	-3	0.1	-2	0.2	-2	0.2	-1	0.3	-1	0.3	0.0	0.4
0.5	54.8	52.3	55.4	52.0	54.5	51.0	54.7	50.9	53.9	50.4	54.5	50.9	54.5	51.4	56.4	53.5	59.4	57.8
1	54.0	52.8	54.8	52.9	54.4	52.2	54.3	51.8	53.3	50.7	53.0	50.2	52.0	49.2	52.3	49.3	53.1	50.5
1.5	53.1	52.5	53.8	52.7	53.6	52.3	53.4	51.9	52.6	50.9	52.0	50.1	50.8	48.8	50.3	48.0	49.9	47.6
2	52.5	52.2	52.9	52.3	52.8	52.0	52.7	51.7	52.0	50.9	51.4	50.1	50.2	48.8	49.2	47.6	48.1	46.4
3	51.5	51.4	51.7	51.4	51.6	51.3	51.5	51.0	51.0	50.4	50.4	49.7	49.3	48.6	48.2	47.3	46.6	45.6
4	50.4	50.3	50.4	50.4	50.4	50.2	50.2	50.0	49.8	49.5	49.3	49.0	48.5	48.1	47.4	46.9	45.8	45.2
5	49.0	49.0	49.1	49.0	49.0	48.9	48.9	48.7	48.6	48.4	48.1	48.0	47.5	47.2	46.6	46.3	45.1	44.8

Table 3. $\omega(\alpha, \beta = 0, \lambda_0 = \infty, \lambda)$ (in degrees)

α λ	-8	-6	-4	-2	0.0	0.2	0.4	0.6	0.8
0.05	39.8	42.4	45.8	48.9	52.0	55.5	59.2	63.6	70.0
0.1	44.3	45.2	47.2	49.5	52.0	55.1	58.4	62.7	68.5
0.2	48.7	48.3	49.3	50.4	52.0	54.2	57.0	60.6	66.3
0.3	50.8	50.2	50.6	51.1	52.0	53.6	55.7	58.7	64.0
0.4	51.8	51.6	51.4	51.5	52.0	53.1	54.6	57.1	61.9
0.5	52.4	52.3	52.0	51.8	52.0	52.7	53.7	55.8	60.1
0.6	52.7	52.7	52.3	52.0	52.0	52.4	53.0	54.6	58.3
0.7	53.1	52.9	52.6	52.2	52.0	52.1	52.5	53.6	56.8
0.8	53.1	53.1	52.8	52.3	52.0	51.9	52.0	52.8	55.5
0.9	53.2	53.2	52.9	52.4	52.0	51.8	51.7	52.1	54.3
1	53.1	53.2	52.9	52.5	52.0	51.7	51.4	51.5	53.3
1.2	53.0	53.2	53.0	52.5	52.0	51.5	50.9	50.6	51.5
1.4	52.9	53.1	53.0	52.6	52.0	51.4	50.6	50.0	50.2
1.6	52.8	53.1	52.9	52.6	52.0	51.3	50.5	49.5	49.2
1.8	52.8	53.0	52.8	52.6	52.0	51.3	50.3	49.2	48.4
2	52.7	52.9	52.8	52.5	52.0	51.3	50.3	49.0	47.8
3	52.4	52.5	52.6	52.4	52.0	51.4	50.3	48.7	46.4
4	52.3	52.4	52.4	52.3	52.0	51.4	50.4	48.9	46.2
5	52.2	52.3	52.3	52.2	52.0	51.5	50.7	49.2	46.3
6	52.1	52.2	52.2	52.2	52.0	51.6	50.9	49.6	46.6
7	52.1	52.2	52.2	52.2	52.0	51.7	51.1	49.8	47.0
8	52.1	52.1	52.2	52.1	52.0	51.7	51.1	50.1	47.3
9	52.1	52.1	52.1	52.1	52.0	51.8	51.2	50.3	47.6
10	52.1	52.1	52.1	52.1	52.0	51.8	51.3	50.3	47.9

$$K_I = \frac{P}{\sqrt{2hA}} \cos \omega + \frac{M}{\sqrt{2h^3I}} \sin \omega$$

$$K_{II} = \frac{P}{\sqrt{2hA}} \sin \omega - \frac{M}{\sqrt{2h^3I}} \cos \omega. \quad (12)$$

The nondimensional effective cross-section, A , and moment of inertia, I , of the composite beam consisting of the film and spalled portion of the substrate can be found in Appendix A. This special case was derived in Drory *et al.* (1988) with different notations, and these authors were able to find an approximate value of ω in the following way. For the film and substrate with *identical* material, i.e. $\alpha = \beta = 0$, ω is obviously independent of λ . The ω for this case can be extracted from the solution presented in Thouless *et al.* (1987), which is

Table 4. $\omega(\alpha, \beta = 0, \lambda_0 = 20, \lambda)$ (in degrees)

α λ	-8	-6	-4	-2	0.0	0.2	0.4	0.6	0.8
1	53.0	53.1	52.9	52.6	52.2	51.8	51.5	51.7	53.6
2	52.5	52.7	52.7	52.4	51.9	51.2	50.2	49.0	48.1
3	52.3	52.4	52.4	52.2	51.8	51.2	50.2	48.7	46.9
4	51.9	52.0	52.0	51.9	51.6	51.0	50.1	48.7	46.6
5	51.6	51.7	51.7	51.6	51.3	50.8	50.1	48.8	46.6
6	51.3	51.3	51.3	51.2	51.0	50.6	49.9	48.7	46.6
7	50.8	50.8	50.8	50.7	50.5	50.2	49.6	48.5	46.5
8	50.3	50.3	50.3	50.2	50.0	49.7	49.2	48.2	46.4
9	49.7	49.7	49.7	49.6	49.4	49.2	48.6	47.9	46.2

Table 5. $\omega(\alpha, \beta = 0, \lambda_0 = 10, \lambda)$ (in degrees)

$\alpha \backslash \lambda$	-0.8	-0.6	-0.4	-0.2	0.0	0.2	0.4	0.6	0.8
0.05	39.9	42.4	45.6	48.9	52.2	55.5	59.1	63.3	70.0
0.1	44.3	45.0	47.0	49.5	52.2	55.1	58.5	62.4	67.9
0.2	48.8	48.4	49.1	50.4	52.1	54.3	56.9	60.4	65.6
0.3	50.8	50.2	50.4	51.0	52.1	53.5	55.6	58.5	63.3
0.4	51.8	51.3	51.2	51.4	52.0	52.9	54.4	56.8	61.2
0.5	52.3	52.0	51.7	51.7	51.9	52.5	53.5	55.4	59.4
0.6	52.6	52.4	52.1	51.9	51.9	52.1	52.8	54.3	57.8
0.7	52.8	52.6	52.3	52.0	51.9	51.9	52.3	53.4	56.4
0.8	52.8	52.8	52.5	52.2	51.9	51.7	51.8	52.6	55.1
0.9	52.9	52.9	52.6	52.3	51.9	51.6	51.5	51.9	54.1
1	52.9	52.9	52.7	52.3	51.9	51.4	51.2	51.4	53.1
1.2	52.8	52.9	52.7	52.3	51.8	51.2	50.7	50.5	51.6
1.4	52.6	52.8	52.6	52.2	51.7	51.2	50.4	49.9	50.4
1.6	52.5	52.6	52.5	52.1	51.6	50.9	50.1	49.4	49.4
1.8	52.3	52.5	52.4	52.0	51.5	50.8	49.9	49.0	48.7
2	52.2	52.3	52.2	51.9	51.4	50.7	49.8	48.8	48.1
3	51.4	51.4	51.4	51.1	50.7	50.0	49.1	47.9	46.6
4	50.4	50.4	50.3	50.0	49.7	49.2	48.4	47.3	45.8
5	49.0	49.1	48.9	48.8	48.5	48.0	47.4	46.5	45.1
6	47.5	47.5	47.4	47.2	46.8	46.4	45.9	45.4	44.2

$\omega = 52.14^\circ$ ($\omega = 52.0^\circ$ from the present analysis). This ω value was taken, with some further justification, for film and substrate of *different* materials, i.e. with $\omega = 52.14^\circ$, (12) becomes

$$\begin{aligned}
 K_I &= 0.434 \frac{P}{\sqrt{Ah}} + 0.558 \frac{M}{\sqrt{Ih^3}} \\
 K_{II} &= 0.558 \frac{P}{\sqrt{Ah}} - 0.434 \frac{M}{\sqrt{Ih^3}}.
 \end{aligned} \quad (13)$$

Comparison of $\omega = 52.14^\circ$ with those ω values listed in Table 1 for $\alpha, \beta \neq 0$ suggests that eqn (13) is a good approximation provided that the film is not too stiff and the crack depth is not too small. We propose that the approximation $\omega = 52^\circ$ can even be taken for finite substrates in eqn (11) according to the values listed in Tables 1–5. As a matter of fact, most of our applications below were first done with this simplification and then the crude results were refined using the more accurate values of ω in those tables.

3. STEADY-STATE CRACKING DEPTH AND DECOHESION NUMBER

As mentioned before, the steady-state cracking position is determined by enforcing $K_{II} = 0$ at the crack tip. From (11) this leads to

$$\frac{\cos(\omega + \gamma)}{\sin \omega} = \sqrt{\frac{V}{U}} \frac{Ph}{M}. \quad (14)$$

For a given film/substrate system, i.e. prescribed α, β and λ_0 , under a given combination of load, Ph/M , the solution of λ to eqn (14) gives the steady-state cracking depth. This depth is then substituted into (11) to calculate K_I . Finally by letting K_I equal to K_{Ic} , the toughness of the substrate, one can determine the critical combination of loads.

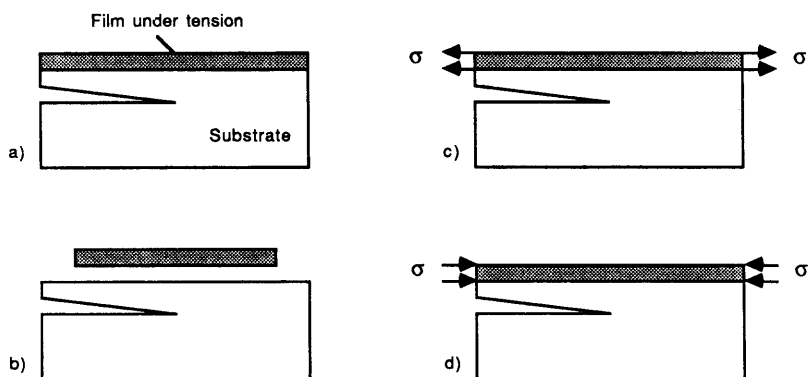


Fig. 3. Equivalent edge load for misfit stress. (a) There is a misfit strain across the film/substrate interface. (b) Cut along the interface. (c) Stretch and paste; no misfit strain is present across the film. (d) The equivalent edge load.

The general nature of the edge load combination of the structure in Fig. 2a provides the flexibility to simulate various practical problems. As an example, cracking driven by residual tensile stress in the film (Fig. 3a) is to be considered in detail. Here σ is the misfit stress in the film relative to the substrate, i.e. σ equals the film stiffness, $8/c_1$, times the misfit strain. The "cut and paste" technique indicates that the crack tip stress field induced by the misfit stress σ is exactly the same as that by the edge loads shown in Fig. 3d. The stress intensity factors can be computed using the solution to the problem in Fig. 2a if the following identification is made:

$$P_1 = P_3 = \sigma h, \quad M_1 = \sigma h^2(\tfrac{1}{2} + \lambda - \Delta), \quad M_3 = \sigma h^2(\tfrac{1}{2} + \lambda_0 - \Delta_0). \quad (15)$$

The reduced loads in Fig. 2c are obtained from (4), i.e.

$$P = \sigma h[1 - C_1 - C_2(\tfrac{1}{2} + \lambda_0 - \Delta_0)], \quad M = \sigma h^2[(\tfrac{1}{2} + \lambda - \Delta) - C_3(\tfrac{1}{2} + \lambda_0 - \Delta_0)]. \quad (16)$$

The energy release rate can be computed from the general formula (5). One may obtain a symmetric form for this special case directly from Fig. 2a by taking the difference between strain energy stored in the composite beams per unit width per unit length far behind and far ahead of the crack tip, i.e.

$$G = \frac{c_2}{16} \sigma^2 h \left[\frac{1}{A} + \frac{(\lambda - \Delta + 1/2)^2}{I} - \frac{1}{A_0} - \frac{(\lambda_0 - \Delta_0 + 1/2)^2}{I_0} \right]. \quad (17)$$

The steady-state cracking depth, λ , is solved from (14) for various α and λ_0 (β is taken to be zero). The results are plotted in Figs 4 and 5. It is remarkable that the solution is so

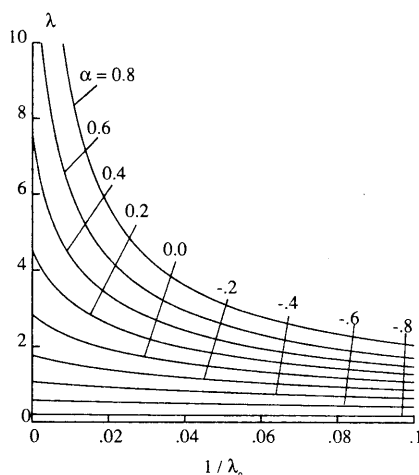


Fig. 4. Steady-state cracking depth as a function of film/substrate thickness ratio.

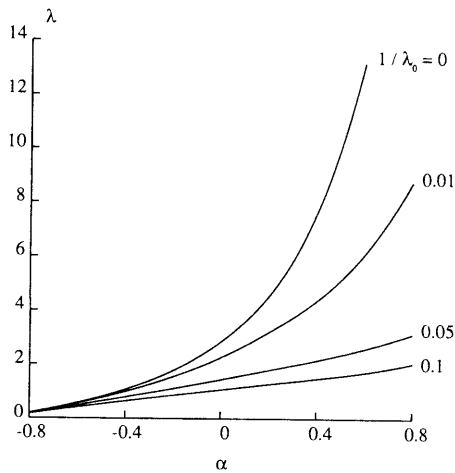


Fig. 5. Steady-state cracking depth as a function of Dundurs' parameter.

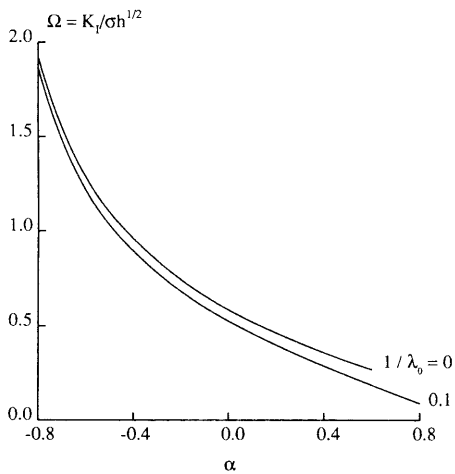


Fig. 6. Decohesion number vs Dundurs' parameter.

sensitive to the substrate/film thickness ratio, λ_0 , even for very large λ_0 , as well as to the Dundurs' parameter α , which is a measure of stiffness ratio of two materials. This critical value of λ is then used to calculate K_I from (11). The decohesion number, $\Omega = K_I/\sigma\sqrt{h}$, is plotted against α for $1/\lambda_0 = 0$ and 0.1 in Fig. 6, providing the critical combination $\sigma\sqrt{h}$ below which steady-state substrate cracking is inhibited if the substrate toughness, K_{Ic} , is known. The decohesion number is somewhat indifferent to the film/substrate thickness ratio in the range $10 < \lambda_0 < \infty$. This clearly indicates that the critical combination $\sigma\sqrt{h}$ is almost a constant for the substrates with the same material but different thickness, as long as the substrates are thick enough. However, the decohesion number is strongly dependent on film/substrate stiffness ratio. The decohesion numbers for some cases are listed in Table 6. A fitting curve for Ω vs Σ relation for a thick substrate ($\lambda_0 = \infty$) is given below

Table 6. Decohesion number $\Omega = \frac{K_I}{\sigma\sqrt{h}}$ vs α and λ_0

$\lambda_0 \backslash \alpha$	-0.8	-0.6	-0.4	-0.2	0.0	0.2	0.4	0.6	0.8
∞	1.92	1.28	0.96	0.75	0.59	0.46	0.36	0.27	0.18
10	1.86	1.21	0.89	0.68	0.53	0.40	0.29	0.19	0.09

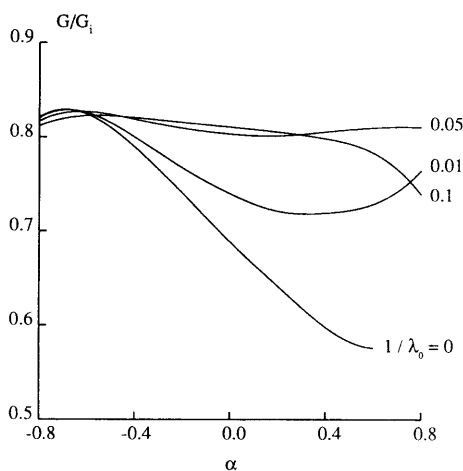


Fig. 7. Energy release rate ratio as a function of Dundurs' parameter.

$$\Omega = \frac{K_I}{\sigma\sqrt{h}} = \begin{cases} (3.50\Sigma - 0.63)^{-0.5}, & 1 \leq \Sigma \leq 10 \\ 0.944\Sigma^{-0.4} - 0.354, & 0.1 \leq \Sigma \leq 1 \end{cases} \quad (18)$$

where Σ is the film/substrate stiffness ratio defined in (2). In the above calculations, ω values are obtained by linear interpolations with respect to $1/\lambda_0$ and λ between those listed in Tables 3–5.

4. ON THE COMPETING CRACKING PATHS

Here we address the tendency of a film/substrate system loaded by a tensile misfit stress in the film to undergo interface cracking in preference to substrate cracking or vice versa. The transient crack path is not analysed. The entire picture will be quite complicated if the transient process is considered, since as illustrated in Fig. 1, cracks often initiate along an interface and then kink out of the interface if the toughness of the substrate is sufficiently low. Here we simply compare the energy release rate available for steady-state substrate cracking with that available for interface cracking. Then, knowing the critical energy release rate for the interface and for the substrate, one can infer which path of cracking is the more likely.

As in Section 3, denote the energy release rate for steady-state substrate cracking (at the depth where $K_{II} = 0$) by G . Denote the energy release rate for a semi-infinite crack along the interface by G_i . The interface crack is mixed mode and a detailed calculation in Suo and Hutchinson (1989a) indicated that the phase angle of the stress intensity factors is around $\pi/4$ for a wide range of film/substrate systems for the tensile misfit stress loading. The energy release rate for the interface crack G_i is given by (17) with $\lambda = 0$ (since G continuously approaches G_i as $\lambda \rightarrow 0^+$). The ratio G/G_i is plotted in Fig. 7 as a function of α for various film/substrate thickness ratios. This ratio is relatively insensitive to the properties of the film/substrate system, varying between 0.55 and 0.83 for most systems.

Let G_c be the substrate toughness and let G_{ic} be the interface toughness (which, in general, can be expected to be a function of the phase angle of the interface stress intensity factors). If

$$\frac{G_c}{G_{ic}} > \frac{G}{G_i} \quad (19)$$

the system is more likely to fracture by interface cracking than substrate cracking. Conversely, if

$$\frac{G_c}{G_{ic}} < \frac{G}{G_i}, \quad (20)$$

substrate cracking will be favored.

5. CONCLUDING REMARKS

The present investigation has provided a relatively complete solution to the problem of a semi-infinite crack parallel to the interface of two bonded infinite elastic layers under general edge loads (Fig. 2a). The energy release rate can be calculated exactly from (5). Exact functional forms of stress intensity factors, eqn (11), are found with only one undetermined dimensionless function $\omega(\alpha, \beta, \lambda_0, \lambda)$, which is then extracted from the numerical solution presented in Appendix B. An approximation $\omega = 52^\circ$ is proposed for those situations in which only relatively crude estimations are desired. The general nature of the problem specified in Fig. 2a makes it convenient to model many problems which might be of interest to scientists and engineers in the field of composite material fabrication, electronic device design, coating protection, etc. One particular problem has been worked out in detail, where substrate cracking depth, and the decohesion number $K_I/\sigma\sqrt{h}$ for the films under residual tension are predicted for various film/substrate systems.

Acknowledgements—This work was supported in part by DARPA University Research Initiative (Subagreement P.O. No. VB38639-0 with the University of California, Santa Barbara, ONR Prime Contract N00014-86-K-0753), by the National Science Foundation under Grant MSM-84-16392, and by the Division of Applied Sciences, Harvard University. Discussions with K. S. Kim have been very helpful.

REFERENCES

- Argon, A. S., Gupta, V., Landis, H. S. and Cornie, J. A. (1989). Intrinsic toughness of interfaces between SiC coatings and substrates of Si or C fibers. *J. Mater. Sci.* **24**, 1406–1412.
- Cannon, R. M., Fisher, R. and Evans, A. G. (1986). Decohesion of thin films from ceramics. *Mat. Res. Soc. Symp. Proc.* **54**, 799–804.
- Charalambides, P. G., Lund, J., Evans, A. G. and McMeeking, R. M. (1989). A test specimen for determining the fracture resistance of bimaterial interfaces. *J. Appl. Mech.* **56**, 77–82.
- Civelek, M. B. (1985). Stress intensity factor for a system crack in an infinite strip. *Fracture Mechanics: Sixteenth Symp. ASTM STP* **868**, 7–26.
- Coker, E. G. and Filon, L. G. N. (1931). *Treatise on Photoelasticity*, p. 130. Cambridge University Press, Cambridge, U.K.
- Drory, M. D., Thouless, M. D. and Evans, A. G. (1988). On the decohesion of residually stressed thin films. *Acta Met.* **36**, 2019–2028.
- Dundurs, J. (1969). Elastic interaction of dislocation with inhomogeneities. *Mathematical Theory of Dislocations*, pp. 70–115. ASME, New York.
- Erdogan, F. and Gupta, G. D. (1971). The stress analysis of multi-layered composites with a flaw. *Int. J. Solids Struct.* **7**, 39.
- Evans, A. G., Drory, M. D. and Hu, M. S. (1988). The cracking and decohesion of thin films. *J. Mater. Res.* **3**, 1043–1049.
- Evans, A. G. and Hutchinson, J. W. (1984). On the mechanics of delamination and spalling in compressed films. *Int. J. Solids Struct.* **20**, 455–466.
- Gruninger, M. F., Lawn, B. R., Farabaugh, E. N. and Wachtman, Jr., J. B. (1987). Measurement of residual stresses in coatings on brittle substrates by indentation fracture. *J. Am. Ceram. Soc.* **70**, 344–348.
- He, M.-Y. and Hutchinson, J. W. (1989). Kinking of a crack out of an interface. *J. Appl. Mech.* **56**, 270–278.
- Hu, M. S., Thouless, M. D. and Evans, A. G. (1988). The decohesion of thin films from brittle substrates. *Acta Met.* **36**, 1301–1307.
- Kim, K. S. and Jiang, W. (1986). Mechanics aspects of the strength of thin film adhesion. IBM Report Contract No. 441614-2.
- Suo, Z. (1989). Singularities interacting with interfaces and cracks. *Int. J. Solids Struct.* (MS 599).
- Suo, Z. and Hutchinson, J. W. (1989a). Interface crack between two elastic layers. To be published in *Int. J. Fracture*.
- Suo, Z. and Hutchinson, J. W. (1988b). On sandwich test specimens for measuring interface crack toughness. *Mater. Sci. Engng* **A107**, 135–143.
- Thouless, M. D., Evans, A. G., Ashby, M. F. and Hutchinson, J. W. (1987). The edge cracking and spall in brittle plates. *Acta Met.* **35**, 1333–1341.

APPENDIX A: ON COMPOSITE BEAMS AND ENERGY RELEASE RATE

The superposition scheme depicted in Figs 2a-c is outlined here. Various quantities are specified in Fig. 2a, where Δ and Δ_0 measuring the position of neutral axes of the corresponding composite layers are given by

$$\Delta = \frac{\lambda^2 + 2\Sigma\lambda + \Sigma}{2(\lambda + \Sigma)}, \quad \Delta_0 = \frac{\lambda_0^2 + 2\Sigma\lambda_0 + \Sigma}{2(\lambda_0 + \Sigma)} \quad (A1)$$

where Σ is the film/substrate stiffness ratio defined by (2). The stresses in the upper beam far behind the crack tip are $\sigma_{22} = \sigma_{12} = 0$ and

$$\sigma_{11}(y) = \begin{cases} -\Sigma\left(\frac{P_1}{hA} + \frac{M_1}{h^3I}y\right), & h(\lambda - \Delta) < y < h(\lambda - \Delta + 1) \\ -\left(\frac{P_1}{hA} + \frac{M_1}{h^3I}y\right), & -h\Delta < y < h(\lambda - \Delta) \end{cases} \quad (A2)$$

where y is measured from the neutral axis, and A and I , the dimensionless effective cross-section and moment of inertia of the beam per unit width, are given by

$$A = \lambda + \Sigma, \quad I = \{\Sigma[3(\Delta - \lambda)^2 - 3(\Delta - \lambda) + 1] + 3\Delta\lambda(\Delta - \lambda) + \lambda^3\}/3. \quad (A3)$$

Similarly, the stresses in the layers far ahead of the crack tip are $\sigma_{22} = \sigma_{12} = 0$ and

$$\sigma_{11}(y_0) = \begin{cases} -\Sigma\left(\frac{P_3}{hA_0} + \frac{M_3}{h^3I_0}y_0\right), & h(\lambda_0 - \Delta_0) < y_0 < h(\lambda_0 - \Delta_0 + 1) \\ -\left(\frac{P_3}{hA_0} + \frac{M_3}{h^3I_0}y_0\right), & -h\Delta_0 < y_0 < h(\lambda_0 - \Delta_0) \end{cases} \quad (A4)$$

where y_0 is measured from the neutral axis at the beam far ahead of the crack tip and

$$A_0 = \lambda_0 + \Sigma, \quad I_0 = \{\Sigma[3(\Delta_0 - \lambda_0)^2 - 3(\Delta_0 - \lambda_0) + 1] + 3\Delta_0\lambda_0(\Delta_0 - \lambda_0) + \lambda_0^3\}/3. \quad (A5)$$

Superposing the structures in Figs 2a and b gives the equivalent loads P and M in Fig. 2c:

$$P = P_1 - C_1P_3 - C_2\frac{M_3}{h}, \quad M = M_1 - C_3M_3 \quad (A6)$$

where

$$C_1 = \frac{A}{A_0}, \quad C_2 = \frac{A}{I_0}[(\lambda_0 - \Delta_0) - (\lambda - \Delta)], \quad C_3 = \frac{I}{I_0}. \quad (A7)$$

The energy release rate for the system in Fig. 2c can be calculated exactly by taking the strain energy stored in the structure per unit width per unit length far behind the crack tip. The result is a positive definite quadratic in P and M which can be written as (5), where

$$\begin{aligned} \frac{1}{U} &= \frac{1}{A} + \frac{1}{\lambda_0 - \lambda} + \frac{12[\Delta + (\lambda_0 - \lambda)/2]^2}{(\lambda_0 - \lambda)^3} \\ \frac{1}{V} &= \frac{1}{I} + \frac{12}{(\lambda_0 - \lambda)^3} \\ \frac{\sin \gamma}{\sqrt{UV}} &= \frac{12[\Delta + (\lambda_0 - \lambda)/2]}{(\lambda_0 - \lambda)^3}. \end{aligned} \quad (A8)$$

APPENDIX B: INTEGRAL EQUATION FORMULATION AND SOLUTION PROCEDURE

A dislocation formulation of the integral equation for the plane elasticity problem of Fig. 2c is used. A general formulation of the integral equations for multilayer problems was presented in Erdogan and Gupta (1971). An edge dislocation solution used as the kernel functions is constructed in Appendix C.

The semi-infinite crack is simulated by an array of continuously distributed edge dislocations along the negative x_1 -axis, with x_i component $b_i(\xi)$ at $x_1 = \xi$, which is to be determined as the solution of the integral equation. The traction-free condition along the crack face results in the integral equation

$$\int_{-\infty}^0 \left[\frac{2}{x - \xi} + F_2(x - \xi) \right] \bar{B}(\xi) d\xi + \int_{-\infty}^0 F_1(x - \xi) B(\xi) d\xi = 0, \quad \text{for } x < 0 \quad (B1)$$

where the first integral is the Cauchy principal value integral, and

$$B(\xi) = \frac{1}{c_2 \pi i} [b_1(\xi) + i b_2(\xi)]. \quad (\text{B2})$$

The complex-valued kernel functions $F_i(\xi)$ are given in Appendix C; they are well-behaved in the whole range $-\infty < \xi < +\infty$, with asymptotes

$$\begin{aligned} F_1(\xi) &= O\left(\frac{1}{\xi^3}\right) \\ F_2(\xi) &= -\frac{2}{\xi} + O\left(\frac{1}{\xi^3}\right) \end{aligned} \quad \text{as } \xi \rightarrow \infty. \quad (\text{B3})$$

We observe that (B1) alone is not sufficient to determine $B(\xi)$ unless the asymptotic behaviors at both the crack tip and infinity are specified.

The relative crack face displacements are related to the dislocation distribution by

$$\delta_1(x) + i\delta_2(x) = \int_x^0 [b_1(\xi) + i b_2(\xi)] d\xi = \pi i c_2 \int_x^0 B(\xi) d\xi, \quad \text{for } x < 0. \quad (\text{B4})$$

Recall the well-known asymptotic expression at the crack tip

$$\delta_2 + i\delta_1 = c_2 K \sqrt{\frac{-\xi}{2\pi}} \quad \text{as } \xi \rightarrow 0^- \quad (\text{B5})$$

where $K = K_I + iK_{II}$ is the complex stress intensity factor. From (B4) and (B5) one can show

$$\bar{K} = (2\pi)^{3/2} \lim_{\xi \rightarrow 0^-} B(\xi) \sqrt{-\xi}. \quad (\text{B6})$$

The behavior of $B(\xi)$ as $\xi \rightarrow -\infty$ can be specified by the displacement fields far behind the crack tip. The results are given below

$$\begin{aligned} \text{Im } [B(\xi)] &= -\frac{P}{8\pi h} \left\{ \frac{1}{A} + \frac{6\Delta}{(\lambda_0 - \lambda)^2} + \frac{4}{\lambda_0 - \lambda} + m \left[\frac{6}{(\lambda_0 - \lambda)^2} - \frac{\Delta}{I} \right] \right\} \\ \text{Re } [B(\xi)] &= -\frac{P}{8\pi h} \left\{ \frac{\sin \gamma}{\sqrt{UV}} + \frac{m}{V} \right\} \frac{\xi}{h} + \text{real constant} \end{aligned} \quad \text{as } \xi \rightarrow -\infty \quad (\text{B7})$$

where $m = M/(Ph)$. The "real constant" is not known *a priori*, but must be determined as part of the integral equation. Since it is the quantity $\omega(\alpha, \beta, \lambda_0, \lambda)$ in (10) that is to be extracted from the integral equation, only one loading combination needs to be solved. In our formulation, P is set m is chosen such that $\text{Re } [B(\xi)]$ remains finite as $\xi \rightarrow -\infty$; that is,

$$m = -\sqrt{\frac{V}{U}} \sin \gamma.$$

Make the change of variables

$$\begin{aligned} x &= \frac{u-1}{u+1}, \quad -1 < u < 1 \\ \xi &= \frac{t-1}{t+1}, \quad -1 < t < 1 \end{aligned}$$

and let

$$\zeta \equiv x - \xi = \frac{2(u-t)}{(u+1)(t+1)}$$

Then with $A(t) \equiv B(\xi)$, the integral equation (B1) can be reduced

$$\int_{-1}^1 \frac{\bar{A}(t)}{u-t} dt + \int_{-1}^1 \frac{F_1(\zeta)A(t) + [1+t+F_2(\zeta)]\bar{A}(t)}{(1+t)^2} dt$$

where the first integral is the Cauchy principal value integral. With one can take the approximation for $A(t)$ as

$$\begin{aligned} P_1 &= \frac{1}{t} \\ P_2 &= \frac{1}{t} \end{aligned}$$

$$A(t) = \left(\frac{1-t}{2} \right)^{-1/2} \left[B(-\infty) + (1+t) \sum_{k=1}^N a_k T_{k-1}(t) \right] \quad (\text{B12})$$

where $\text{Im}[B(-\infty)]$ is specified in (B7) while $\text{Re}[B(-\infty)]$ is an unknown finite number, $T_j(t)$ is the Chebyshev polynomial of the first kind of degree j and the a s are complex coefficients which must be determined in the solution process.

When substituted into (B11), the representation for $A(t)$ leads to an equation of the form

$$\sum_{k=1}^N [a_k I_1(u, k) + \bar{a}_k I_2(u, k)] + \text{Re} \{B(-\infty)\} I_3(u) = I_4(u) \quad (\text{B13})$$

where the terms I_j for $j = 1, 4$ involve integrals such as

$$I_1(u, k) = \int_{-1}^1 F_1(\zeta) T_{k-1}(t) (1+t)^{-1} \left(\frac{1-t}{2} \right)^{-1/2} dt. \quad (\text{B14})$$

These integrals must be evaluated numerically for given values of u and k .

The solution procedure is as follows. Let a set of $2N$ real unknowns be $\text{Re}[B(-\infty)]$ plus the real and imaginary parts of a_k for $k = 1, N$, excluding the real part of a_N (i.e. effectively, $\text{Re}\{a_N\}$ is set to zero). This set of $2N$ unknowns is used to satisfy the real and imaginary parts of (B11) at N Gauss-Legendre points $\{u_i\}$ on the interval $-1 < u < 1$. Once the a s have been determined, the complex stress intensity factor can be computed, using (B6) and (B12), from

$$\bar{K} = (2\pi)^{3/2} \left\{ B(-\infty) + 2 \sum_{k=1}^N a_k \right\}. \quad (\text{B15})$$

The general expression for K in (10) applies to the present case with $P = 1$, $M = mh$, so that

$$K = \frac{\cos \gamma}{\sqrt{2Uh}} e^{i\gamma} e^{i\omega}. \quad (\text{B16})$$

The numerical solution yields both the real and the imaginary parts of K . The magnitude of K is known from the energy release rate and thus provides a consistency check on the accuracy of the solution. The results reported in Tables 1-5 were computed with N between 10 and 15. The consistency check was satisfied to better than 0.1%. It is believed that the accuracy of ω is comparable.

APPENDIX C: AN EDGE DISLOCATION IN COMPOSITE LAYERS

The construction of the dislocation solution used as the kernel in the integral equation (B1) is summarized here. The plane elasticity problem is specified in Fig. C1a. An edge dislocation with components b_1 and b_2 is embedded in medium No. 2 at $(0, -d)$. The entire external boundary is traction-free. The problem is solved by superposing the following two structures

- (i) two bonded half-planes with an edge dislocation at $(0, -d)$ (Fig. C1b) and
- (ii) two bonded layers *without* dislocation (Fig. C1c) but with tractions prescribed along its upper and lower boundaries as the negative of those calculated along $y = h$ and $-H$ in structure (i).

Problems like (i) with point-wise singularity embedded in one of two bonded semi-infinite media can be solved in general by analytical continuation arguments. With $z = x + iy$, two analytic functions $\Phi(z)$ and $\Omega(z)$ used below relate to stress and displacement components by

$$\begin{aligned} \sigma_{xx} + \sigma_{yy} &= 2[\Phi(z) + \bar{\Phi}(z)] \\ \sigma_{yy} + i\sigma_{xy} &= \bar{\Phi}(z) + \Omega(z) + (\bar{z} - z)\Phi'(z) \\ 2\mu \frac{\partial}{\partial x}(u_x - iu_y) &= \kappa \bar{\Phi}(z) - \Omega(z) - (\bar{z} - z)\Phi'(z). \end{aligned} \quad (\text{C1})$$

If the potentials, $\Phi_0(z)$ and $\Omega_0(z)$, for a singularity embedded in an *infinite homogeneous* plane of material No. 2 are known, the potentials for the problem of two bonded half-planes with the same singularity in material No. 2 can be constructed by remarkably simple relations (Suo, 1989):

$$\Phi(z) = \begin{cases} (1+\Lambda)\Phi_0(z), & z \text{ in No. 1} \\ \Phi_0(z) + \Pi\bar{\Omega}_0(z), & z \text{ in No. 2} \end{cases} \quad \Omega(z) = \begin{cases} (1+\Pi)\Omega_0(z), & z \text{ in No. 1} \\ \Omega_0(z) + \Lambda\bar{\Phi}_0(z), & z \text{ in No. 2.} \end{cases} \quad (\text{C2})$$

Here Λ and Π measure the inhomogeneity by

$$\Lambda = \frac{\alpha + \beta}{1 - \beta}, \quad \Pi = \frac{\alpha - \beta}{1 + \beta}. \quad (\text{C3})$$

For an edge dislocation at $z = s$ ($s = -id$ for our case),

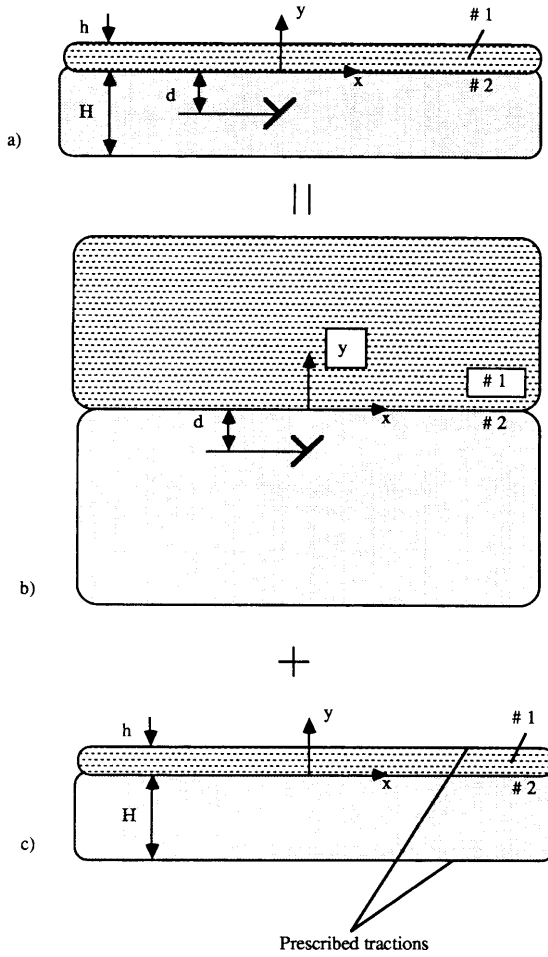


Fig. C1. Construction of the kernel functions.

$$\Phi_0(z) = B \left[\frac{1}{z-s} \right], \quad \Omega_0(z) = B \left[\frac{\bar{s}-s}{(z-s)^2} \right] + \bar{B} \left[\frac{1}{z-s} \right], \quad B = \frac{1}{\pi i c_2} (b_1 + i b_2). \quad (C4)$$

The stresses along $z = \zeta - id$ in Fig. C1b derived from the potentials via (C2) are

$$\sigma_{22}(\zeta, -d) + i\sigma_{12}(\zeta, -d) = \bar{B} \left[\frac{2}{\zeta} + H_2(\zeta) \right] + B H_1(\zeta) \quad (C5)$$

where

$$H_1(\zeta) = \frac{16\pi d^2 \zeta}{(\zeta^2 + 4d^2)^2}, \quad H_2(\zeta) = \frac{(\Lambda + \Pi)\zeta + (\Lambda - \Pi)2id}{\zeta^2 + 4d^2} - \frac{8\pi d^2}{(\zeta - 2id)^3}. \quad (C6)$$

The solution procedure to problem (ii) is similar to that developed in Civelek (1985) for a homogeneous strip. Such multilayer problems can be conveniently solved using Fourier transforms with two real potentials, $U(x, y)$ and $\chi(x, y)$, satisfying (Coker and Filon, 1931)

$$\Delta^2 U = 0, \quad \Delta \chi = 0, \quad \frac{\partial^2 \chi}{\partial x \partial y} = \frac{1}{4} \Delta U \quad (C7)$$

where $\Delta = \partial^2/\partial x^2 + \partial^2/\partial y^2$. The stresses and displacements can be derived from

$$\sigma_{xx} = \frac{\partial^2 U}{\partial^2 y}, \quad \sigma_{yy} = \frac{\partial^2 U}{\partial^2 x}, \quad \sigma_{xy} = -\frac{\partial^2 U}{\partial x \partial y}$$

$$2\mu u_x = -\frac{\partial U}{\partial x} + (\kappa + 1) \frac{\partial \chi}{\partial y}, \quad 2\mu u_y = -\frac{\partial U}{\partial y} + (\kappa + 1) \frac{\partial \chi}{\partial x}.$$

The general approach to the multilayer problems is as follows. For each layer, the solution of $U(x, y)$ can

separated into two parts: one is symmetric in changing x to $-x$, the other is antisymmetric. For the symmetric part, for example, upon satisfying (C7) the two potentials can be represented by Fourier integrals

$$\begin{aligned} U(x, y) &= \int_0^\infty \left\{ \left[\frac{A_1}{\lambda^2} + \frac{A_2}{\lambda} y \right] e^{-\lambda y} + \left[\frac{A_3}{\lambda^2} + \frac{A_4}{\lambda} y \right] e^{i\lambda y} \right\} \cos \lambda x \, d\lambda \\ \chi(x, y) &= \int_0^\infty \frac{1}{2\lambda^2} \{ A_2 e^{-\lambda y} + A_4 e^{i\lambda y} \} \sin \lambda x \, d\lambda. \end{aligned} \quad (C9)$$

The constants A_i are then solved by matching the displacements and tractions along the interface and satisfying the external boundary conditions. The following integrals may be helpful to obtain the Fourier transforms of the tractions on the external boundaries

$$I_n(\lambda, a) = \int_0^\infty \frac{\cos \lambda x}{(x^2 + a^2)^n} dx, \quad J_n(\lambda, a) = \int_0^\infty \frac{x \sin \lambda x}{(x^2 + a^2)^n} dx, \quad (a > 0). \quad (C10)$$

One can easily verify the recursive relations

$$\begin{aligned} I_1 &= \frac{\pi}{2a} e^{-a\lambda}, \quad I_{n+1} = -\frac{1}{2na} \frac{\partial I_n}{\partial a} \\ J_1 &= \frac{\pi}{2} e^{-a\lambda}, \quad J_{n+1} = -\frac{1}{2na} \frac{\partial J_n}{\partial a}. \end{aligned} \quad (C11)$$

Further algebraic details are omitted. The final results are reported below. The stresses along $z = \zeta - id$ in Fig. C1 can be represented by

$$\sigma_{22}(\zeta, -d) + i\sigma_{12}(\zeta, -d) = \bar{B}G_2(\zeta) + BG_1(\zeta) \quad (C12)$$

where

$$\begin{aligned} G_1(\zeta) &= [Q_2(\zeta) - R_1(\zeta)] + i[Q_1(\zeta) + R_2(\zeta)] \\ G_2(\zeta) &= [Q_2(\zeta) + R_1(\zeta)] + i[R_2(\zeta) - Q_1(\zeta)] \end{aligned} \quad (C13)$$

where the Q s and R s are defined by the Fourier integrals

$$\begin{aligned} Q_1(\zeta) &= \int_0^\infty \{ [-C_1 + \lambda d C_2] e^{i\lambda d} + [-C_3 + \lambda d C_4] e^{-i\lambda d} \} \cos \lambda \zeta \, d\lambda \\ R_1(\zeta) &= \int_0^\infty \{ [-C_1 + (1 + \lambda d) C_2] e^{i\lambda d} + [C_3 + (1 - \lambda d) C_4] e^{-i\lambda d} \} \sin \lambda \zeta \, d\lambda \\ Q_2(\zeta) &= \int_0^\infty \{ [-D_1 + \lambda d D_2] e^{i\lambda d} + [-D_3 + \lambda d D_4] e^{-i\lambda d} \} \sin \lambda \zeta \, d\lambda \\ R_2(\zeta) &= \int_0^\infty \{ [D_1 - (1 + \lambda d) D_2] e^{i\lambda d} - [D_3 + (1 - \lambda d) D_4] e^{-i\lambda d} \} \cos \lambda \zeta \, d\lambda \end{aligned}$$

where the C s and D s are solved from the linear algebraic equations

$$\begin{bmatrix} P_1 \\ P_2 \end{bmatrix} \begin{bmatrix} C_1 & D_1 \\ C_2 & D_2 \\ C_3 & D_3 \\ C_4 & D_4 \end{bmatrix} = \begin{bmatrix} X_1 & Y_1 \\ X_2 & Y_2 \\ X_3 & Y_3 \\ X_4 & Y_4 \end{bmatrix}. \quad (C14)$$

Here

$$\begin{aligned} P_1 &= \begin{bmatrix} -e^{-\lambda h} & -\lambda h e^{-\lambda h} & -e^{i\lambda h} & -\lambda h e^{i\lambda h} \\ -e^{-\lambda h} & (1 - \lambda h) e^{-\lambda h} & e^{i\lambda h} & (1 + \lambda h) e^{i\lambda h} \end{bmatrix} \frac{1}{1 - \alpha} \begin{bmatrix} 1 - \beta & \beta & -(\alpha - \beta) & \beta \\ 0 & 1 + \beta & -2(\alpha - \beta) & -(\alpha - \beta) \\ -(\alpha - \beta) & -\beta & 1 - \beta & -\beta \\ 2(\alpha - \beta) & -(\alpha - \beta) & 0 & 1 + \beta \end{bmatrix} \\ P_2 &= \begin{bmatrix} -e^{i\lambda H} & \lambda H e^{i\lambda H} & -e^{-\lambda H} & \lambda H e^{-\lambda H} \\ -e^{i\lambda H} & (1 + \lambda H) e^{i\lambda H} & e^{-\lambda H} & (1 - \lambda H) e^{-\lambda H} \end{bmatrix} \end{aligned}$$

$$\begin{aligned} X_1 &= -\left\{ -\frac{\Lambda - \Pi}{2} - [(1 + \Pi)(h + d) + (\Lambda - \Pi)h]\lambda \right\} e^{-\lambda(h+d)} \\ X_2 &= -\left\{ \frac{2 + \Lambda + \Pi}{2} - [(1 + \Pi)(h + d) + (\Lambda - \Pi)h]\lambda \right\} e^{-\lambda(h+d)} \end{aligned}$$

$$\begin{aligned}
X_3 &= - \left\{ \left[-\frac{\Lambda - \Pi}{2} + \Pi(H-d)\lambda - 2\Pi Hd\lambda^2 \right] e^{-(H+d)\lambda} + (H-d)\lambda e^{-(H-d)\lambda} \right\} \\
X_4 &= - \left\{ \left[\frac{\Lambda + \Pi}{2} - \Pi(H+d)\lambda + 2\Pi Hd\lambda^2 \right] e^{-(H+d)\lambda} + [1 - (H-d)\lambda] e^{-(H-d)\lambda} \right\} \\
Y_1 &= - \left\{ \frac{2 + \Lambda + \Pi}{2} + [(1 + \Pi)(h+d) + (\Lambda - \Pi)]\lambda \right\} e^{-(h+d)\lambda} \\
Y_2 &= + \left\{ \frac{\Lambda - \Pi}{2} - [(1 + \Pi)(h+d) + (\Lambda - \Pi)]\lambda \right\} e^{-(h+d)\lambda} \\
Y_3 &= - \left\{ \left[\frac{\Lambda + \Pi}{2} + \Pi(H+d)\lambda + 2\Pi Hd\lambda^2 \right] e^{-(H+d)\lambda} + [1 + (H-d)\lambda] e^{-(H-d)\lambda} \right\} \\
Y_4 &= + \left\{ \left[\frac{\Lambda - \Pi}{2} + \Pi(H-d)\lambda + 2\Pi Hd\lambda^2 \right] e^{-(H+d)\lambda} + (H-d)\lambda e^{-(H-d)\lambda} \right\}.
\end{aligned}$$

The solution to the problem in Fig. C1a is obtained by superposing (C5) and (C12), i.e. for the infinite composite strip, the stresses at $(\zeta, -d)$ induced by the dislocation at $(0, -d)$ are given by

$$\sigma_{22}(\zeta, -d) + i\sigma_{12}(\zeta, -d) = \bar{B} \left[\frac{2}{\zeta} + F_2(\zeta) \right] + BF_1(\zeta) \quad (\text{C15})$$

and $F_i = H_i + G_i$.